

Supporting Information

Oxygen-regulated carbon quantum dots as efficient metal-free electrocatalyst for nitrogen reduction

*Yaqian Han,^{‡a} Xiaoteng Ding,^{‡a} Jingrui Han,^a Yanfeng Fang,^a Zhaoyong Jin,^a Wenhan Kong,^a and Chuangwei Liu^{*a,b}*

^a Institute of Biomedical Engineering, College of Life Sciences, Qingdao University, Qingdao 266071, China.

^b Key Lab for Anisotropy and Texture of Materials, School of Materials Science and Engineering, Northeastern University, Shenyang 110819, China

Corresponding author: chliua@dtu.dk

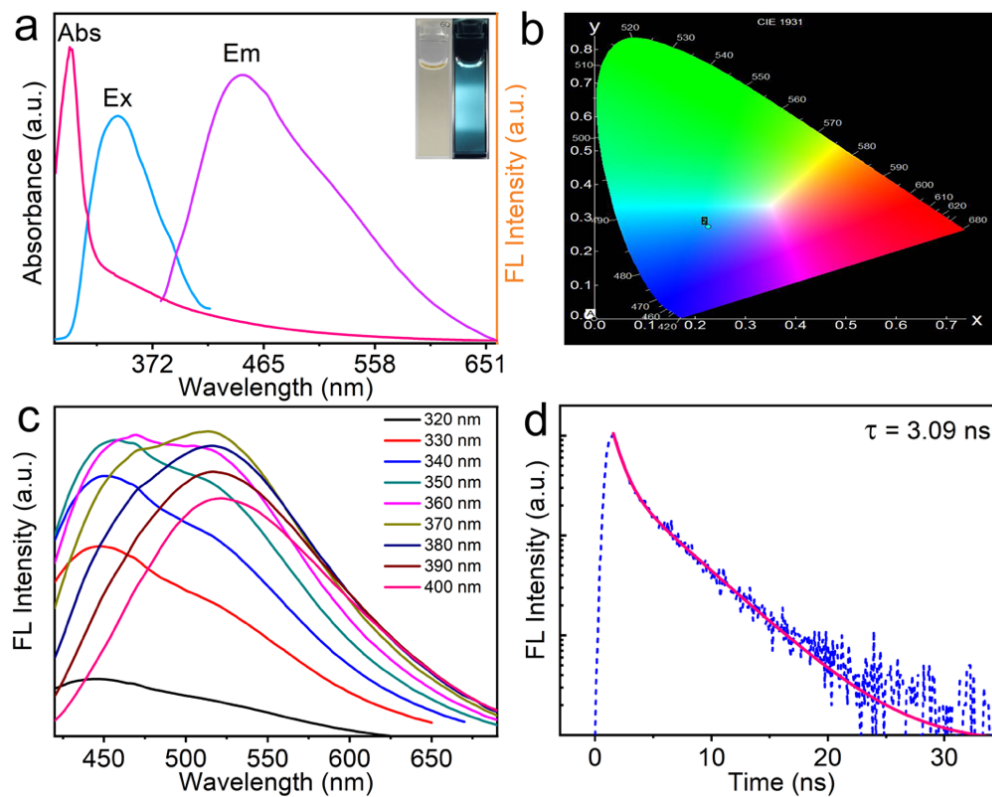


Figure S1. (a) UV–Vis absorption spectrum (Abs), the maximum excitation (Ex) and emission (Em) of CQDs. Photographs of CQDs suspensions under room light (inset, left) and under 365 nm UV light (inset, right), respectively. (b) The luminous colour of CQDs in 1931 CIE chromaticity chart. (c) Em spectra of CQDs at excitation wavelengths varying from 320 to 400 nm. (d) The FL decay spectra and fitting curves of CQDs suspension.

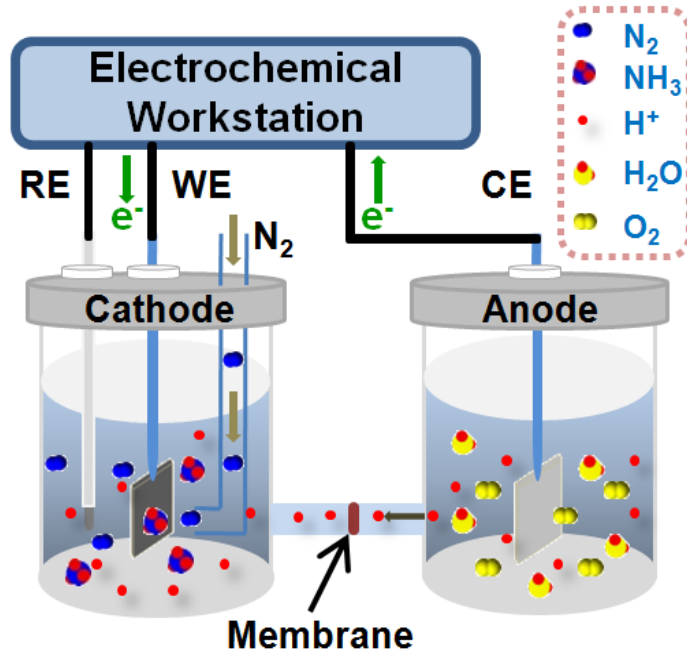


Figure S2. Schematic diagram for electrocatalytic NRR.

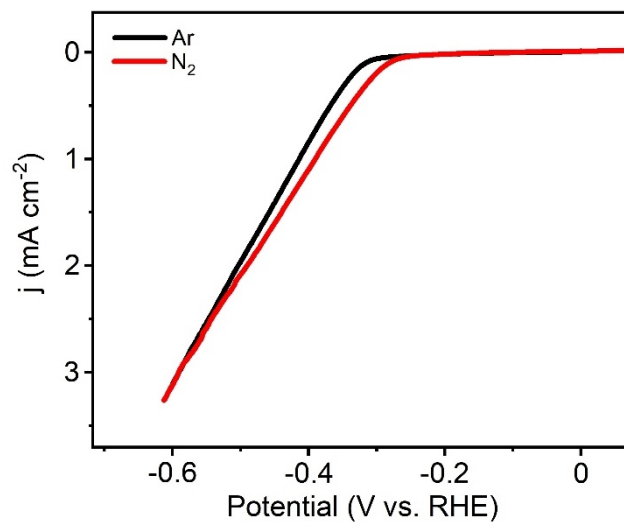


Figure S3. LSV curves of the electrode in Ar- and N₂-saturated 0.1M HCl.

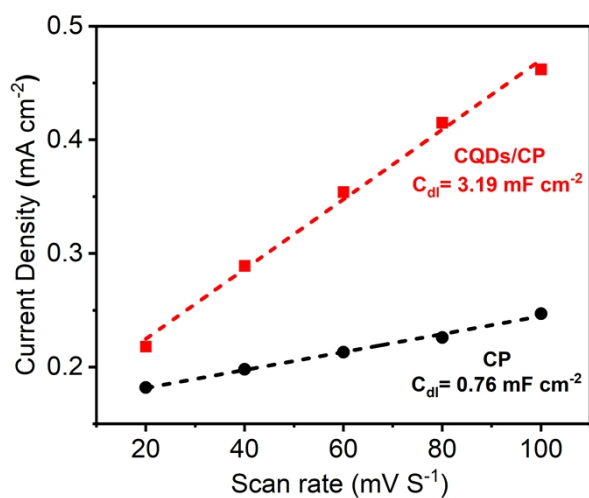


Figure S4. Linear relationship of CQDs/CP and CP between absolute value of current density difference and scanning rate.

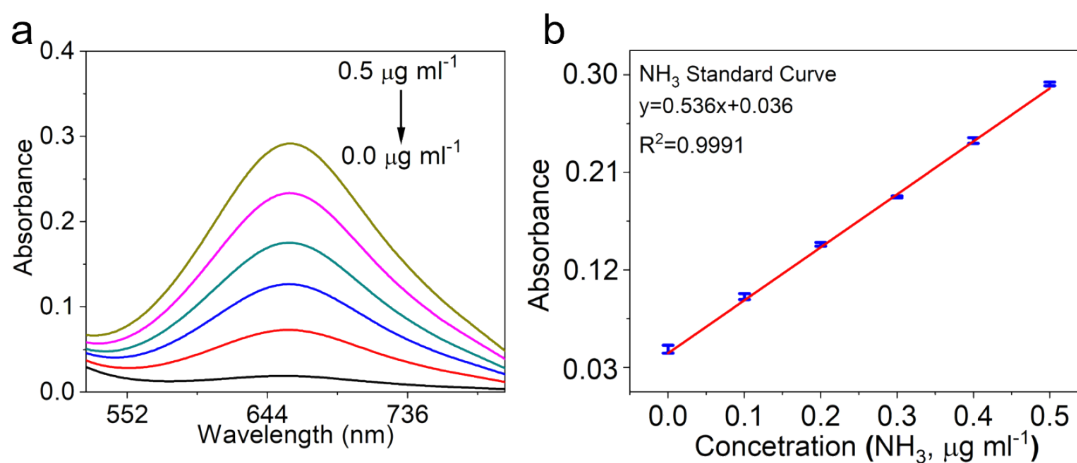


Figure S5. (a) UV-Vis absorption spectra of indophenol assays with NH₃ ions after incubated for 2 h at room temperature. (b) Calibration curve used for estimation of NH₃ (error bar=SD, n=3).

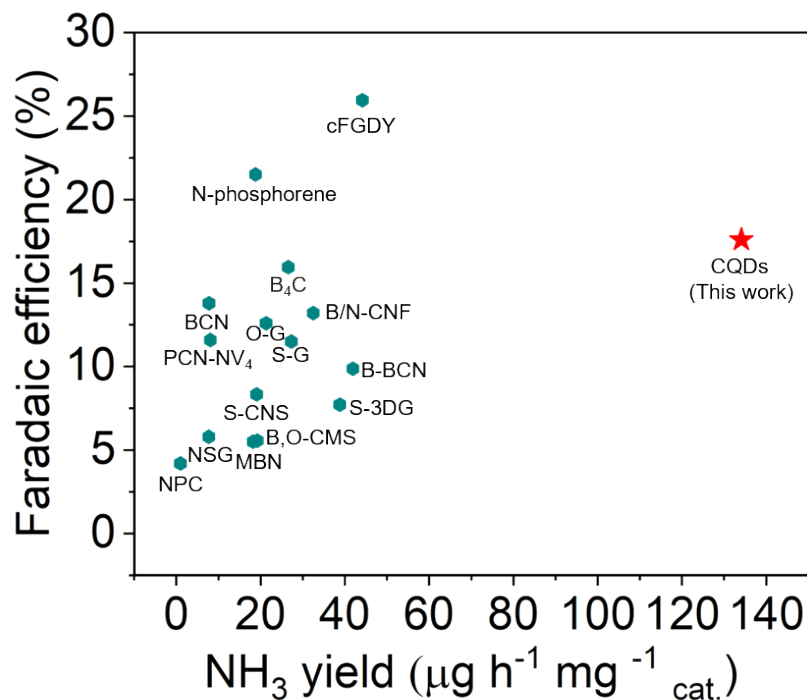


Figure S6. Recent progress of electrochemical NH_3 synthesis under ambient conditions.

Table S1. Comparison of the NH_3 electrosynthesis activity for CQDs with some reported metal-free NRR electrocatalysts at ambient conditions.

Catalysts	NH_3 yields	FE	References
N-phosphorene	$18.79 \mu\text{g h}^{-1} \text{mg}^{-1}_{\text{cat.}}$	21.51%	10.1039/d0ta03237a
S-Doped three-dimensional graphene	$38.81 \mu\text{g h}^{-1} \text{mg}^{-1}_{\text{cat.}}$	7.72%	10.1039/c9dt04827h
MBN	$18.2 \mu\text{g h}^{-1} \text{mg}^{-1}_{\text{cat.}}$	5.5%	10.1039/c8nr10401h
cFGDY	$44.14 \pm 4.54 \mu\text{g h}^{-1} \text{mg}^{-1}_{\text{cat.}}$	$25.95 \pm 2.6\%$	10.1039/d0nh00287a
B/N-CNF	$32.5 \mu\text{g h}^{-1} \text{mg}^{-1}_{\text{cat.}}$	13.2%	10.1039/c9ta06076f
B/O-CMS	$19.2 \mu\text{g h}^{-1} \text{mg}^{-1}_{\text{cat.}}$	5.57%	10.1016/j.ijhydene.2020.09.187
B-CN	$41.9 \mu\text{g h}^{-1} \text{mg}^{-1}_{\text{cat.}}$	9.87 %	10.1016/j.apcatb.2020.119622
N, S co-doped graphene	$7.7 \mu\text{g h}^{-1} \text{mg}^{-1}_{\text{cat.}}$	5.8%	10.1007/s10853-019-03538-0
PCN-NV ₄	$8.09 \mu\text{g h}^{-1} \text{mg}^{-1}_{\text{cat.}}$	11.59%	10.1002/anie.201806386
B ₄ C	$26.57 \mu\text{g h}^{-1} \text{mg}^{-1}_{\text{cat.}}$	15.95%	10.1038/s41467-018-05758-5
S-Doped Carbon Nanospheres	$19.07 \mu\text{g h}^{-1} \text{mg}^{-1}_{\text{cat.}}$	8.34%	10.1002/smt.201800251
BCN	$7.75 \mu\text{g h}^{-1} \text{mg}^{-1}_{\text{cat.}}$	13.79%	10.1002/smll.201805029
Oxygen-doped graphene	$21.3 \mu\text{g h}^{-1} \text{mg}^{-1}_{\text{cat.}}$	12.6%	DOI: 10.1039/c9cc01999e
sulfur-doped graphene	$27.3 \mu\text{g h}^{-1} \text{mg}^{-1}_{\text{cat.}}$	11.5%	10.1039/c9cc00602h
NPC	$0.97 \mu\text{g h}^{-1} \text{mg}^{-1}_{\text{cat.}}$	4.2%	10.1039/c8cc09256g

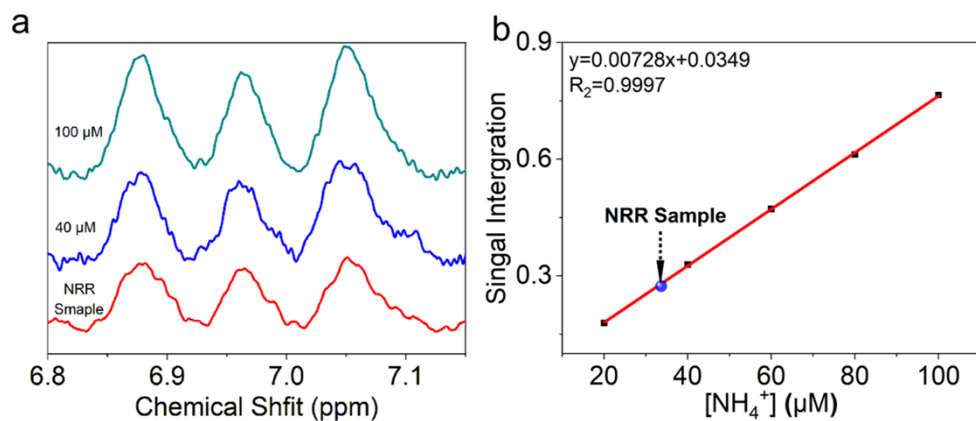


Figure S7. (a) ¹H NMR spectra (600 MHz) of NH₄⁺ produced from the NRR experiment and standard NH₄⁺ samples. (b) Calibration curve of the ¹H NMR signal at 6.97 ppm for standard solutions of NH₄⁺ (20, 40, 60, 80, 100 μM) and the NRR sample.

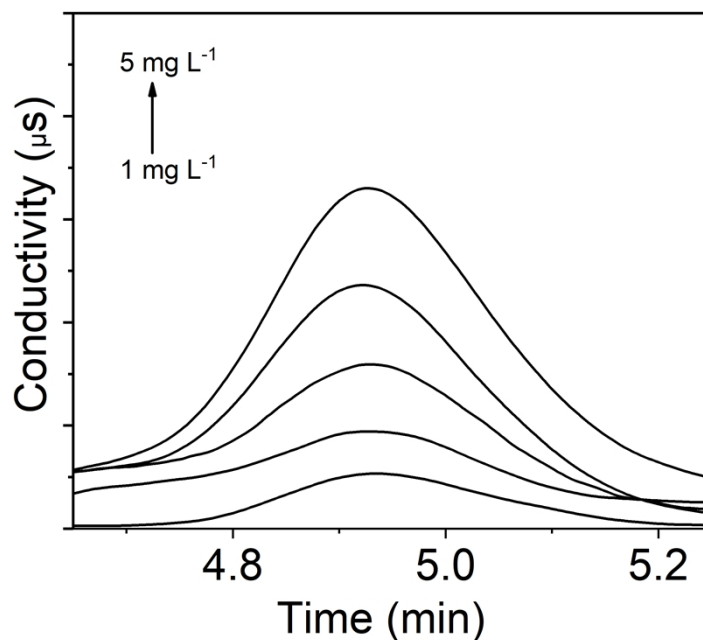


Figure S8. (a-e) Ion chromatography spectra of standard NH₄⁺ samples (a-e) and NH₄⁺ produced from the NRR experiment (f).

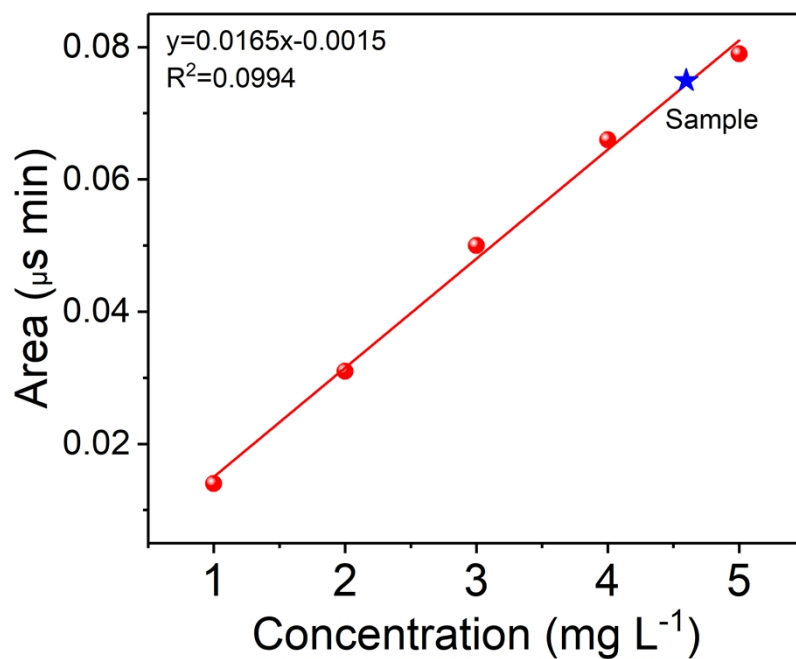


Figure S9. Calibration curve of the Ion chromatography spectra for standard solutions of NH₄⁺ and the NRR sample.

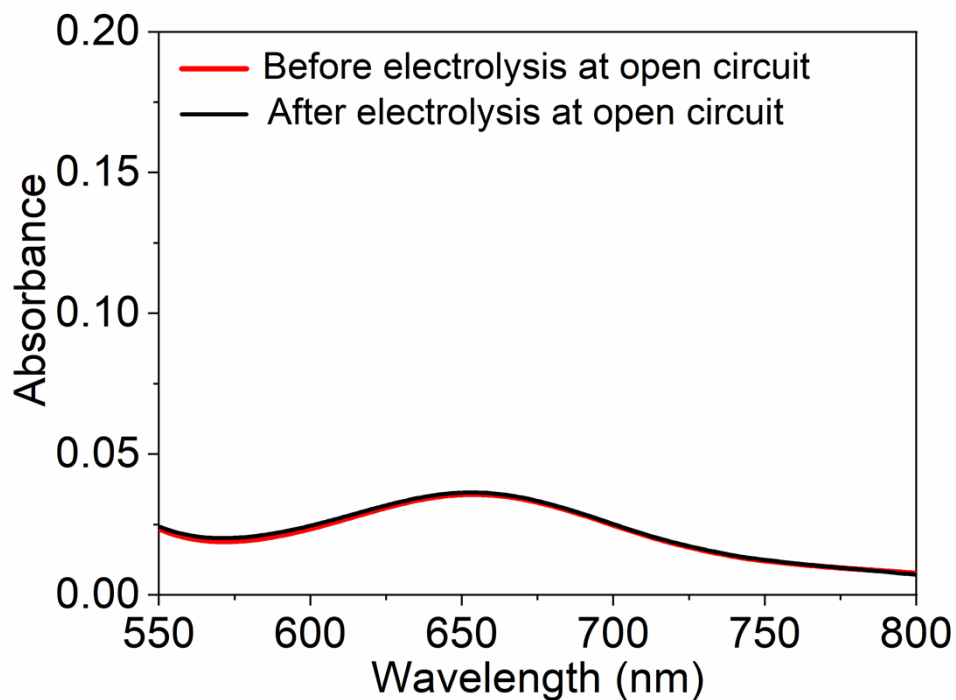


Figure S10. UV-Vis absorption spectra of the electrolytes stained with indicator before and after 2 h electrolysis under open circuit conditions.

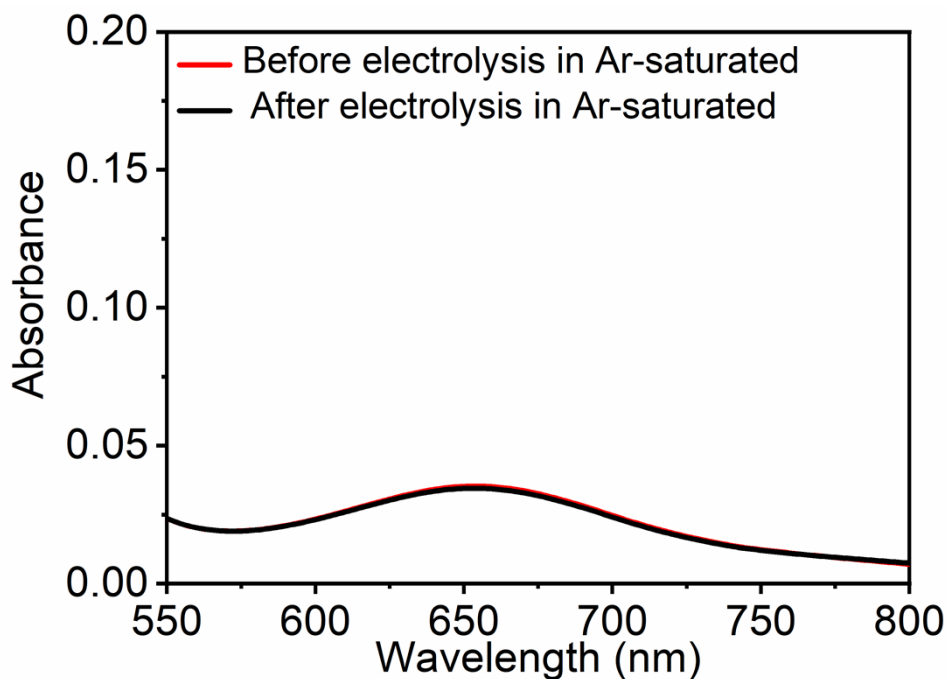


Figure S11. UV-Vis absorption spectra of the electrolyte stained with indicator before and after 2 h electrolysis at the potential of -0.45 V under Ar-saturated solution.

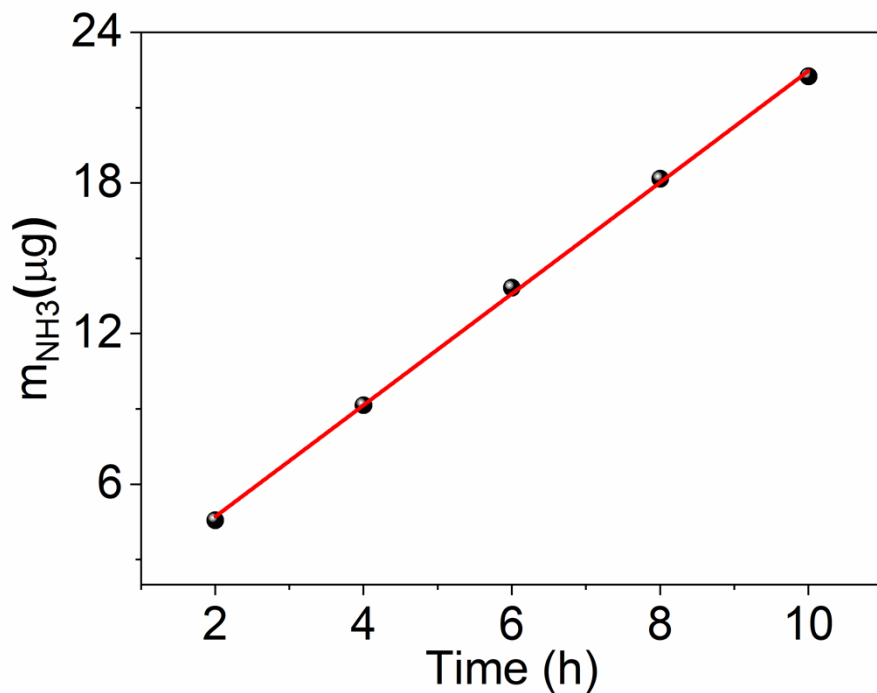


Figure S12. Amount of produced NH_3 vs. time recorded at -0.45 V.

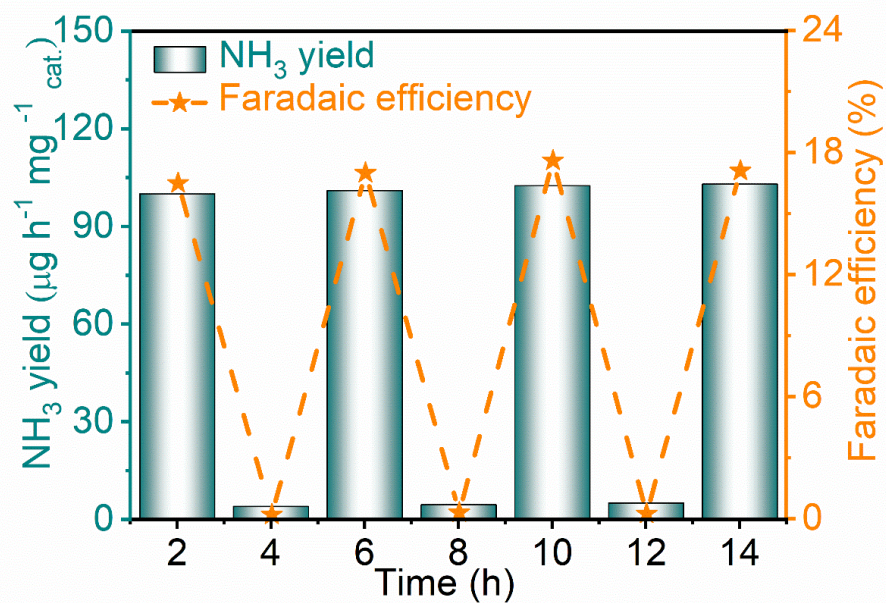


Figure S13. NH_3 yields (left y-axis) and FEs (right y-axis) of CQDs/CP with alternating 2 h cycles between N_2 -saturated and Ar-saturated electrolytes for a total of 14 h at -0.45 V.

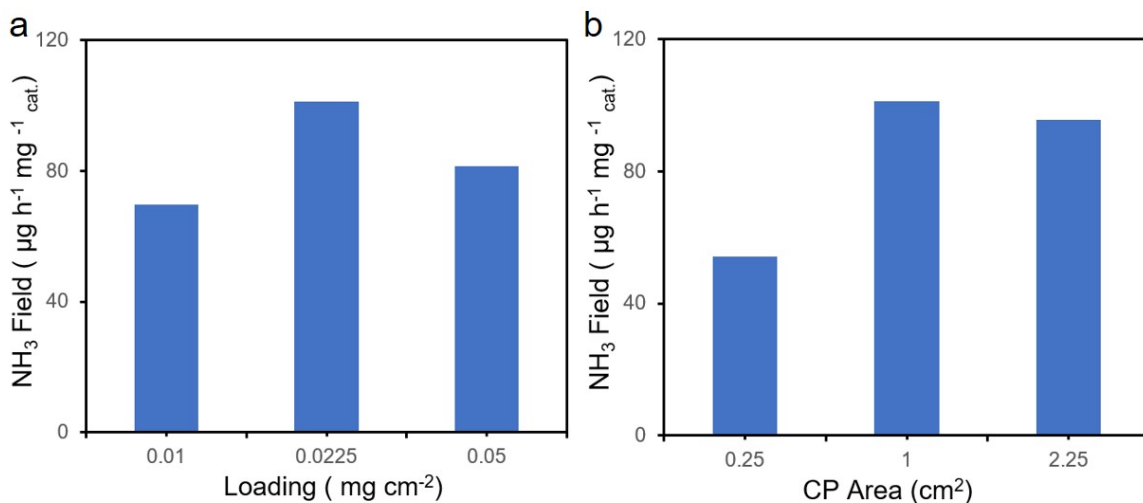


Figure S14. NH_3 yields of CQDs/CP with different loading and different CP area.

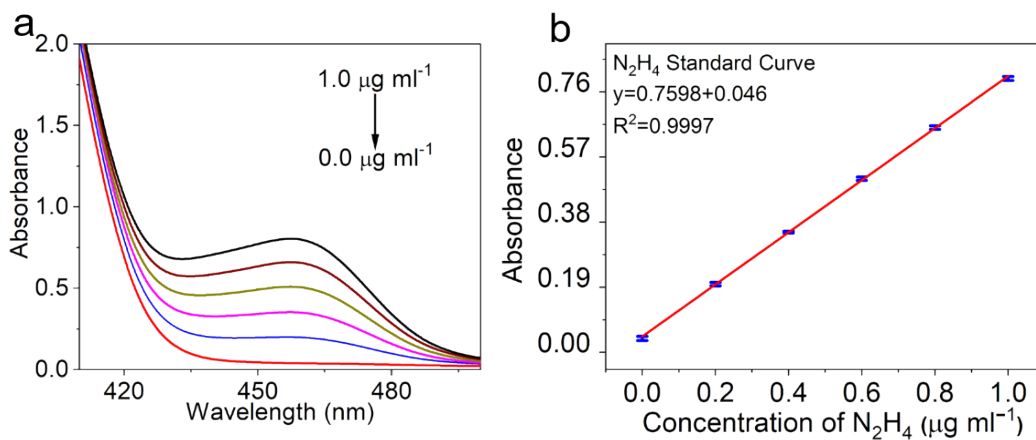


Figure S15. (a) UV-Vis absorption spectra of various N_2H_4 concentrations after incubated for 10 min at room temperature. (b) Calibration curve used for estimation of N_2H_4 concentration (error bar = SD, $n=3$).

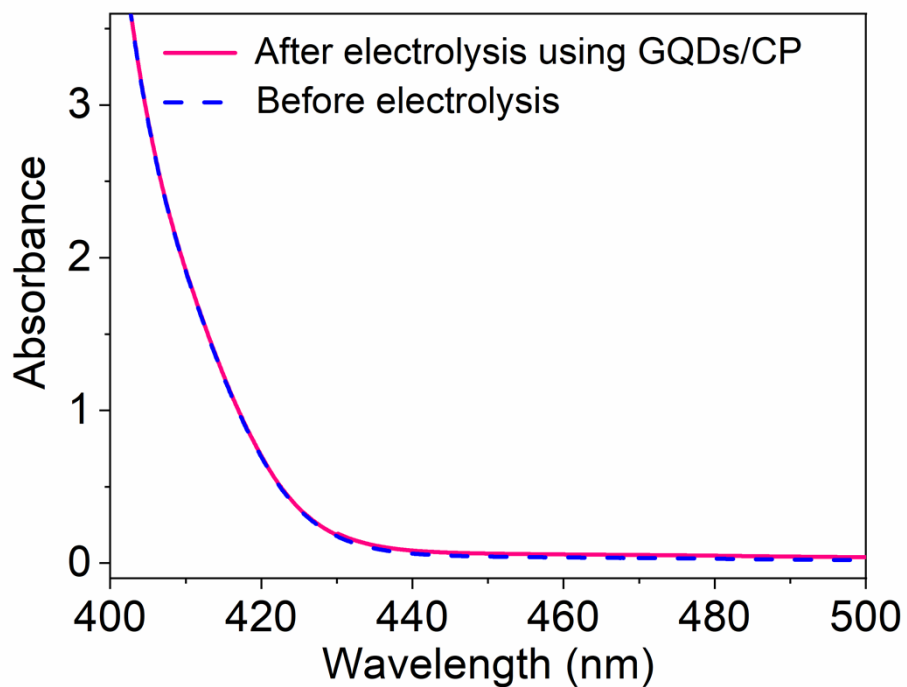


Figure S16. UV-Vis absorption spectra of N_2H_4 before and after 2 h electrolysis in N_2 atmosphere at $-0.45v$.

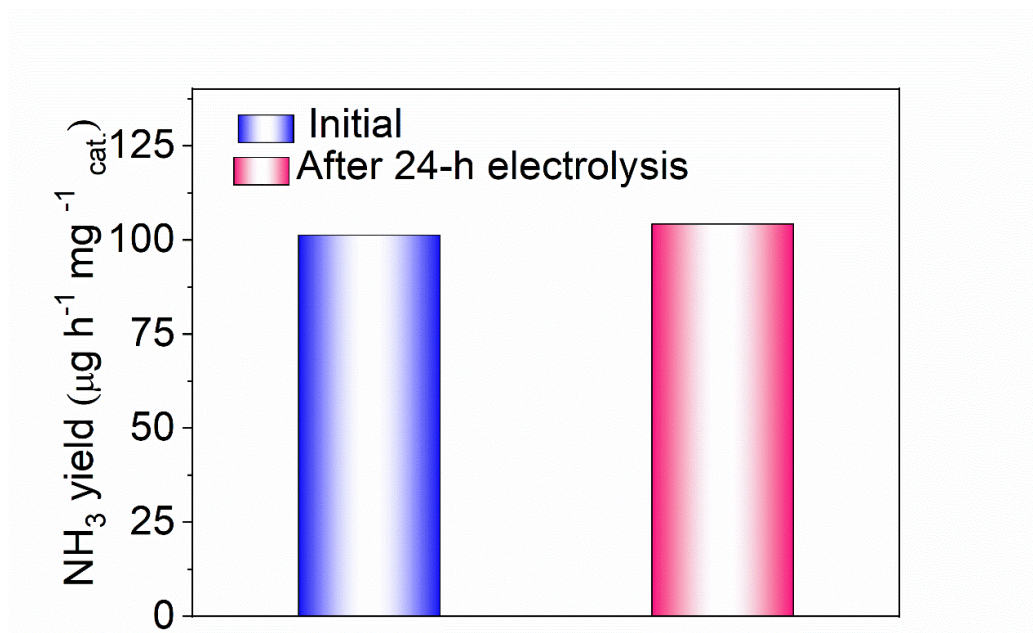


Figure S17. NH_3 yields after electrolysis at $-0.45 V$ for 2 h and 24 h, respectively.

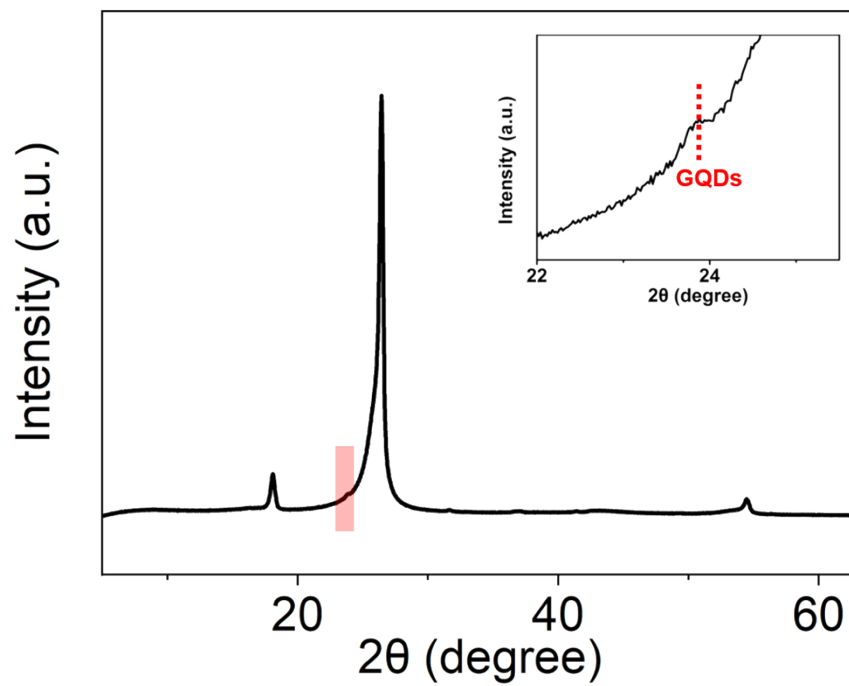


Figure S18. The survey XRD patterns of CQDs-CP after stability test in N_2 -saturated solution.

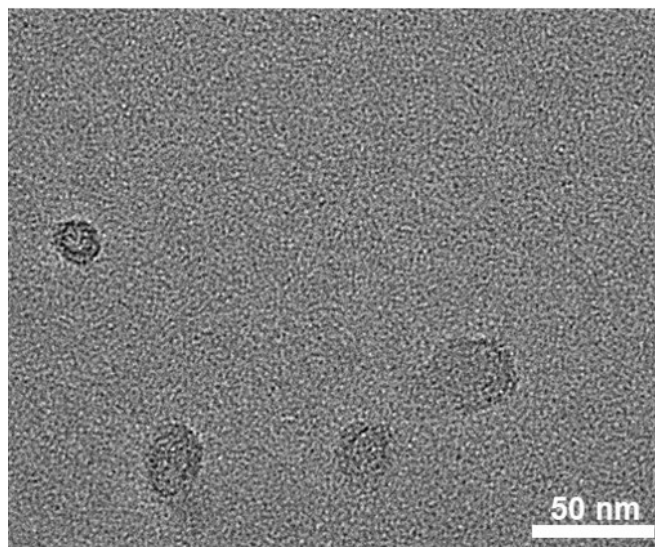


Figure S19. The TEM image of CQDs-CP after stability test in N_2 -saturated solution.

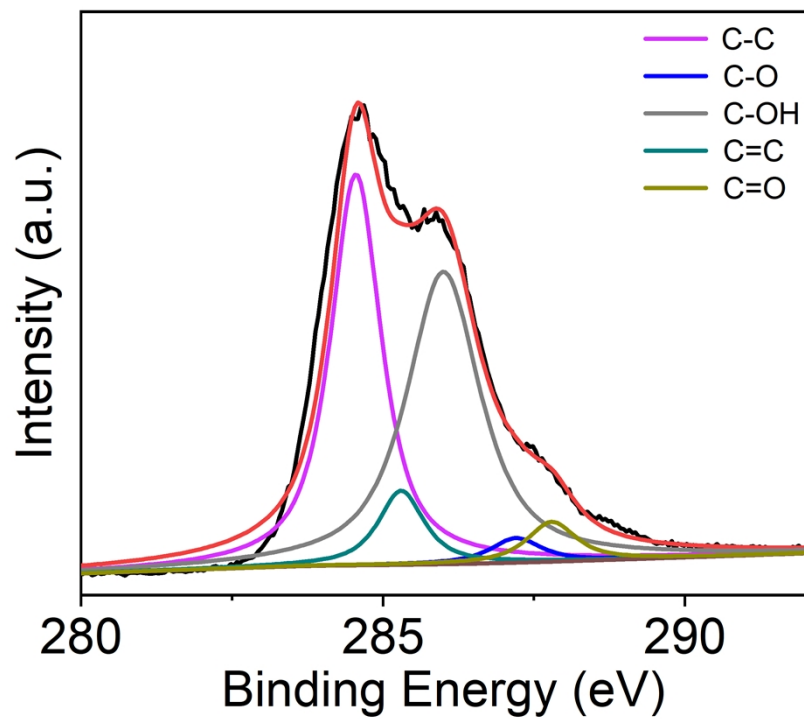


Figure S20. The XPS survey spectrum of CQDs/CP after stability test in N_2 -saturated solution.

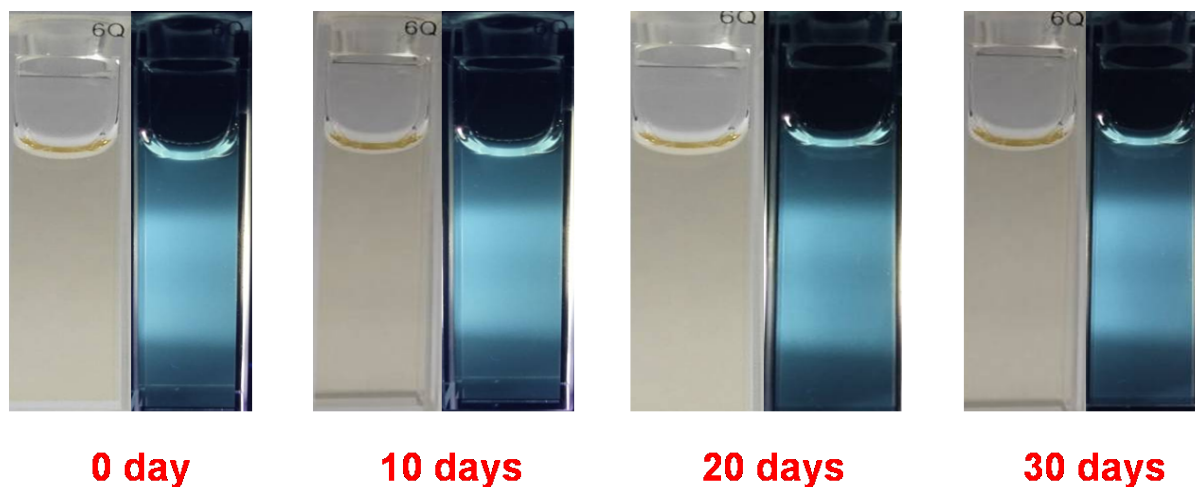


Figure S21. Photographs of CQDs suspensions under room light (left) and under 365 nm UV light (right) after placing 0, 10, 20 and 30 days, respectively.

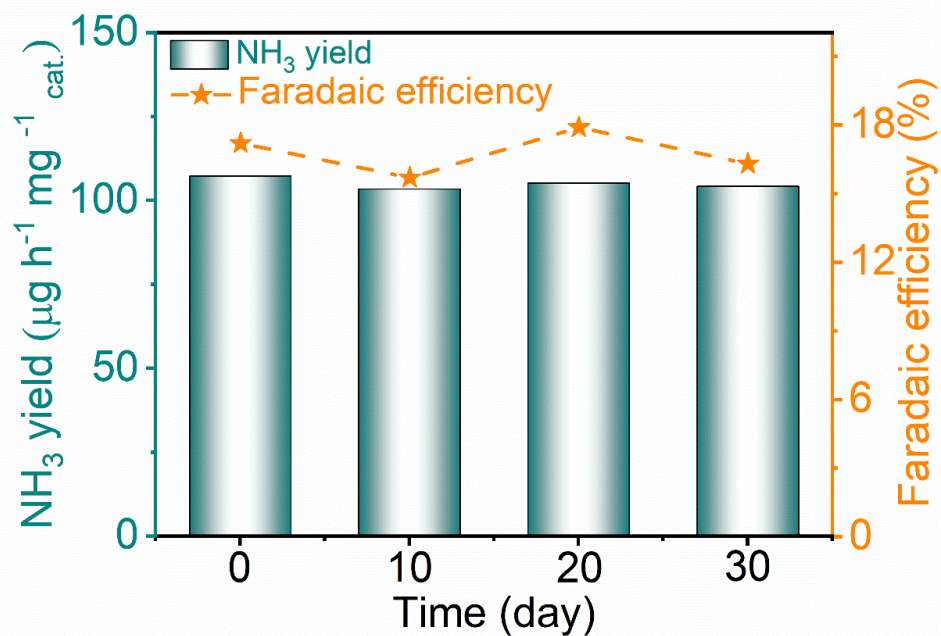


Figure S22. The NH₃ yields and FEs of CQDs at -0.25 V after placing 0, 10, 20, 30 days, respectively.

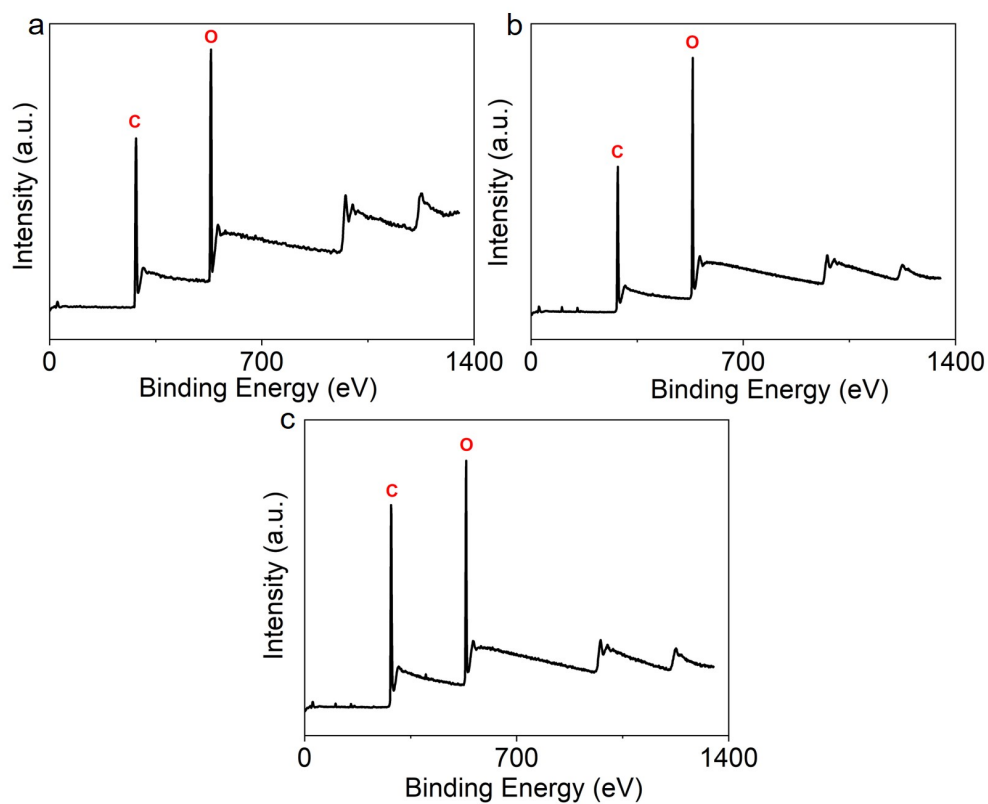


Figure S23. The XPS survey spectrum of C140, C160, and C180, respectively.

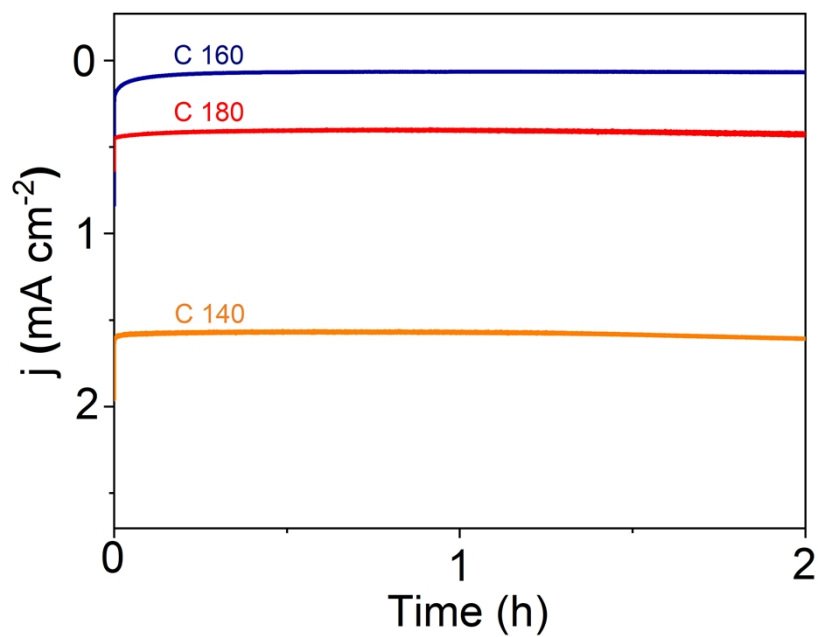


Figure S24. Time-dependent current density curves of C140, C160, and C180.

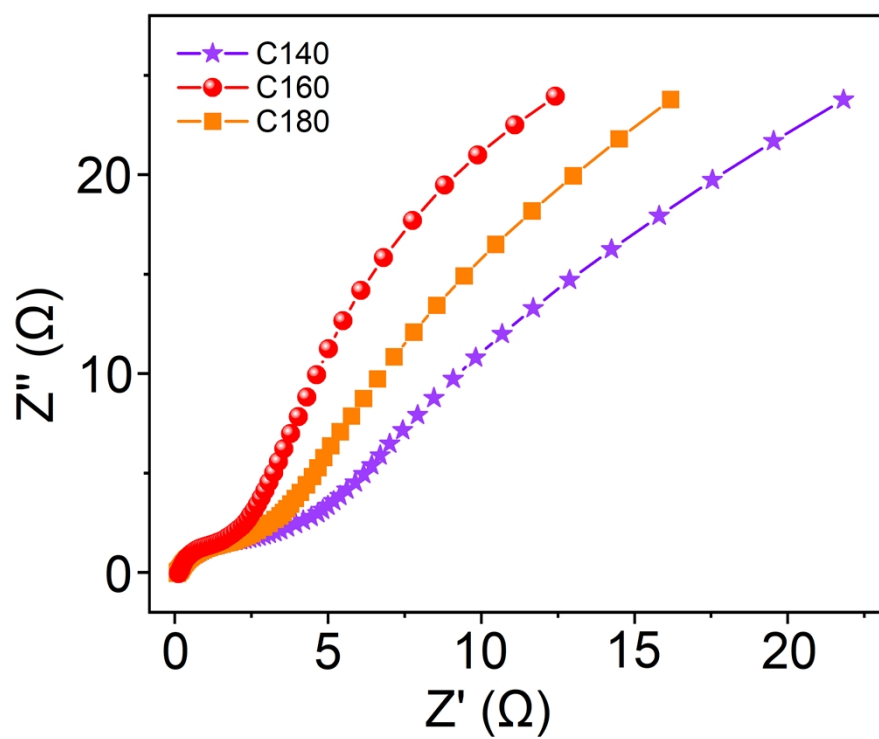


Figure S25. EIS spectra of C140, C160, and C180, respectively.

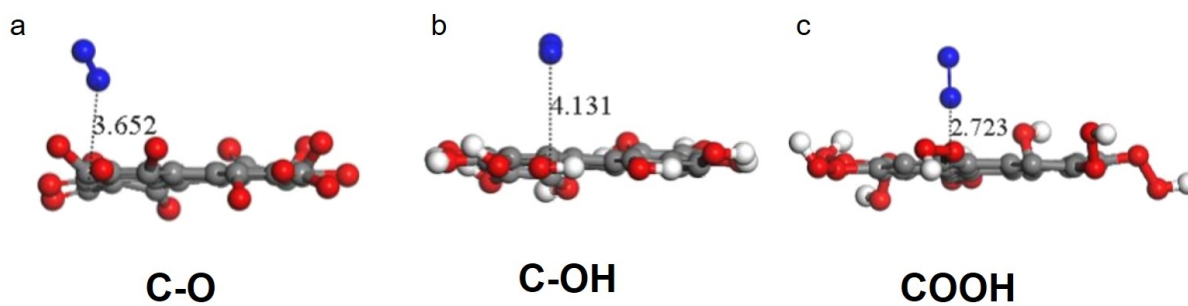


Figure S26. Optimized structures the N_2 -adsorbed configuration on oxygen-containing functional groups of CQDs C-O (a), C-OH (b) and COOH (c), respectively.

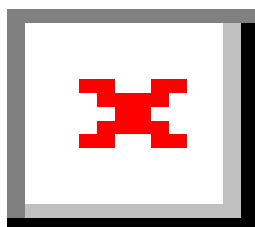


Figure S27. Optimized structure the N_2 -adsorbed configuration on site 3 of CQDs.

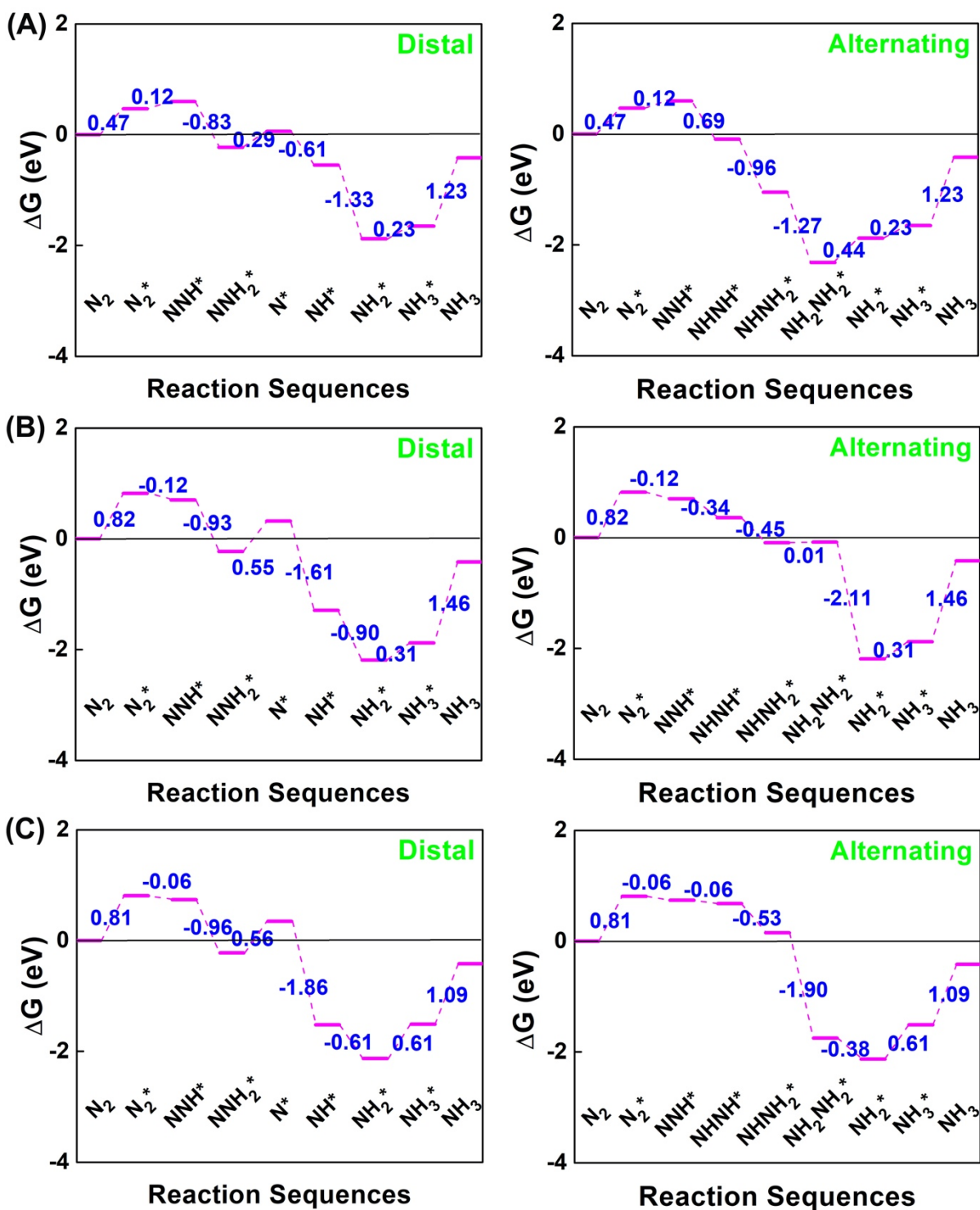


Figure S28. Free energy scheme for the NRR on the (a) site 1, (b) site 2 and (c) site 4, respectively.

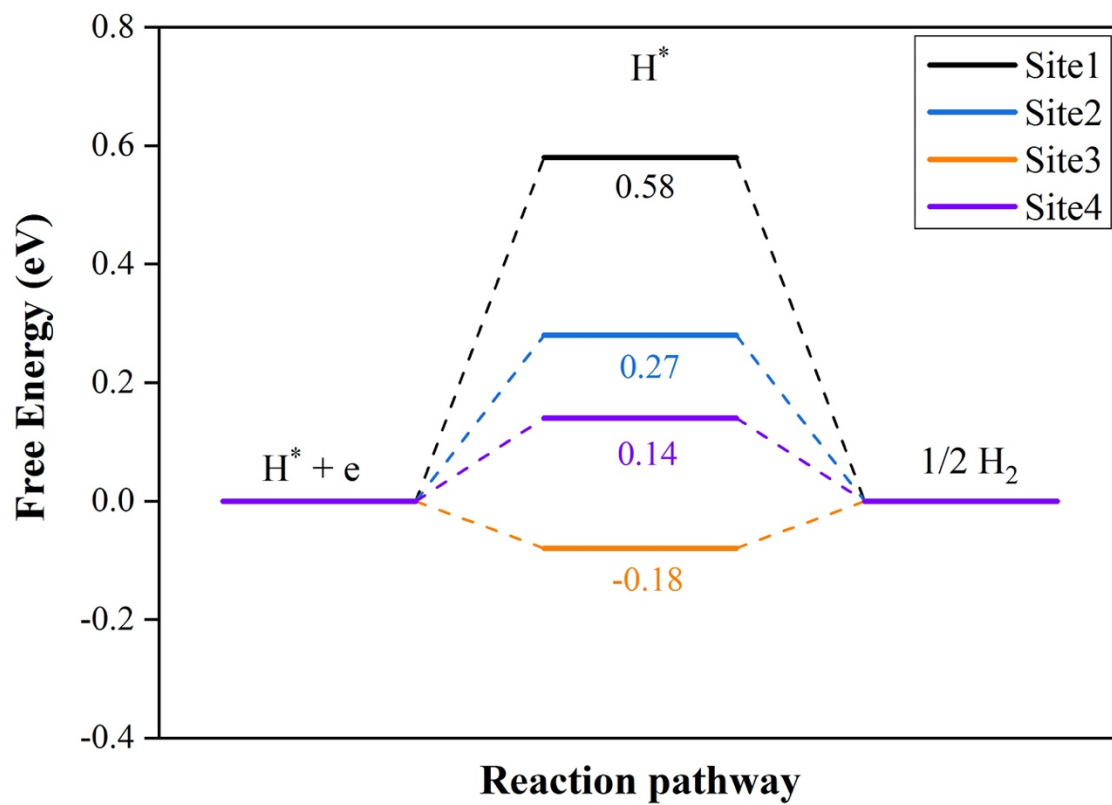


Figure S29. The calculated free-energy diagram for the formation of H_2 at equilibrium on four sites of CQDs, respectively.

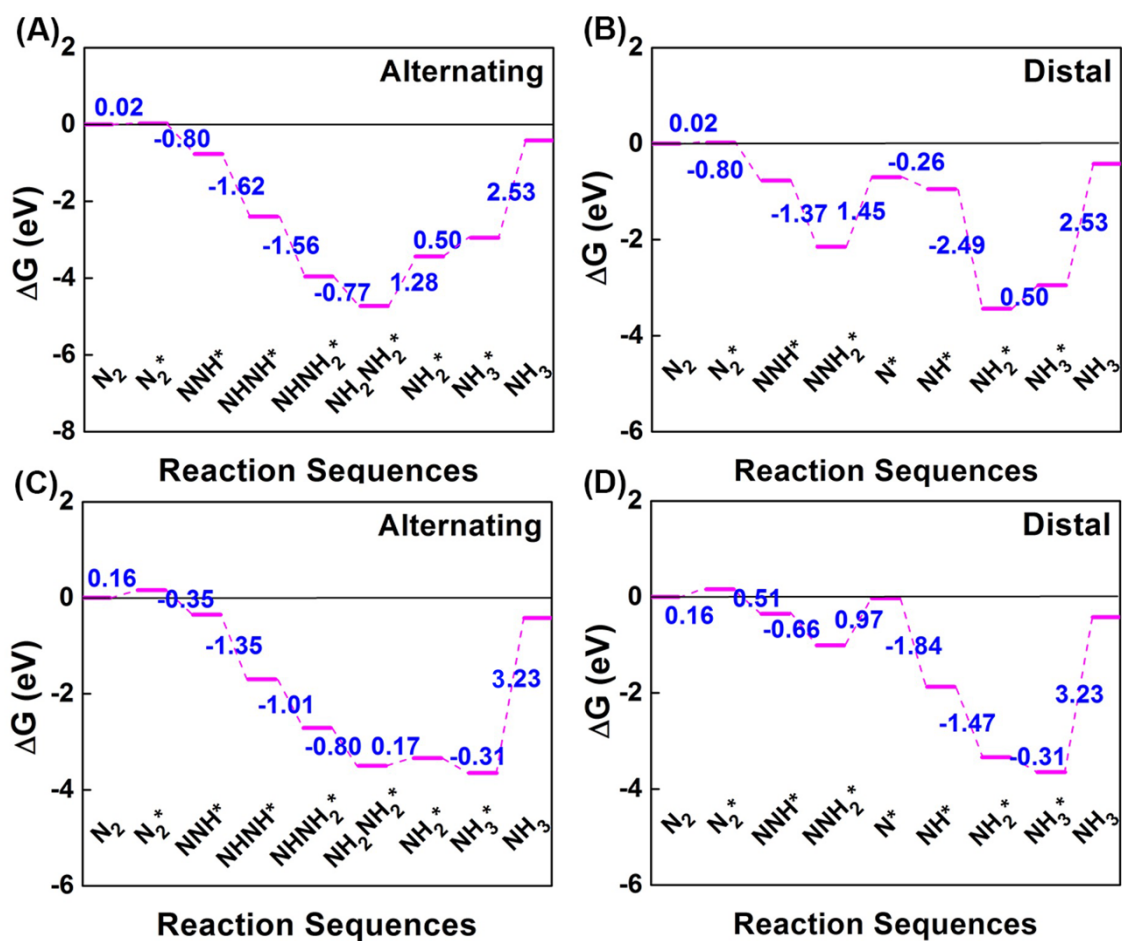


Figure S30. Free energy scheme for the NRR of CQDs. The alternating (a) and the (b) distal hydrogenation route of NRR on the 10% oxygen coverage on the surface of CQDs. The alternating (c) and the (d) distal hydrogenation route of NRR on the 20% oxygen coverage on the surface of CQDs.